Simulation of transonic airfoil flow with a zonal RANS-LES method

B. Roidl, M. Meinke, and W. Schröder
Institute of Aerodynamics, RWTH Aachen University
Wüllnerstraße 5a, 52062 Aachen, Germany

Abstract

In this paper a zonal RANS-LES approach is presented in which the regions with attached boundary-layers are computed via RANS and the regions with separated flows by using LES. The transition from RANS to LES takes place in an overlapping region between the RANS and LES zone. Two different turbulent inflow generation methods are presented and coupled with a controlled forcing ansatz which enable a fast and smooth transition from two-dimensional RANS- to the three-dimensional unsteady LES solutions. Both approaches require local Reynolds shear stresses of a RANS solution which is located upstream of the LES. The inflow generation methods are validated for boundary-layer flows and the fully coupled zonal approach is applied to a transonic flow over an airfoil including a shock boundary-layer interaction.

1 Introduction

Most of all industrial CFD applications at high Reynolds numbers are nowadays based on solutions of the Reynolds averaged Navier-Stokes (RANS). The reasons for their application are obvious: they are simple to apply and computationally efficient. Therefore, they are used for the flow analysis at design and off-design conditions, for optimization and for cases where experimental data may not be easily obtained. However, it is known that solutions provided by one- or two equation eddy viscosity models are not reliably predicting complex flow cases [1]. Although various modifications and new concepts of turbulence modelling, i.e. algebraic Reynolds stress models, non-linear eddy-viscosity closures, etc., were proposed over the last decades, the optimum universal model has not been found yet.

The alternatives to RANS modelling are Direct- and Large-Eddy Simulation (DNS and LES). Todays available computer resources, however, prevent these methods to become standard simulation tools for high Reynolds number flows. Since in many applications complex flow regions are limited to a smaller part of the domain, hybrid methods, combining the computational efficiency of of RANS with the higher accuracy of LES or DNS should in principle be able to provide better results at minimized additional costs.

An overview of hybrid and zonal RANS/LES approaches is given in [2]. There are at least two major techniques to couple RANS with LES in hybrid computations. The first approach uses a continuous turbulence model, which switches from RANS to LES mode in a unified domain, such as the detached eddy simulation (DES) proposed in [3],[4]. The other technique uses two separate computational domains which are linked via an overlapping zone where the transition from RANS to LES and vice versa occurs. This technique is also applied and further investigated with respect to the interface conditions in this paper. Within this method the turbulent flow properties at the LES inlet have to be prescribed by using information from the RANS solution. There are three distinct types of such inflow boundary conditions [5]: recycling a plane of flow characteristics downstream of the inflow plane; instantaneous flow fields from precursor simulations or fluctuations (random or physical) which are superimposed on a mean velocity profile. The latter method is well suited for the interface problem because the fluctuations, that contain the moments of the RANS simulation, could be either generated by local forcing, or computed separately and superimposed on a mean velocity profile that is also provided by the upstream RANS solution.

Recent applications that apply the synthetic eddy method (SEM) by Jarrin *et al.* [6] or that are based on the synthetic, homogeneous turbulence method by Kraichnan [7], which was extended to inhomogeneous flows by Smirnov *et al.* [8] and Batten *et al.* [9] suffer from long transition lengths for realistic turbulence to be generated. Following the idea of Keating [10] this development region can be significantly shortened by combining synthetic turbulence generation methods (STGM) with controlled forcing [11] that is applied downstream of the LES inlet, which will be demonstrated in this

paper.

The article is organized as follows: In section 2, the numerical methods of the flow solver and the synthetic turbulence generation methods are described. Subsequently, in section 3, the results are presented. First, the various STGM are compared for different configurations in zero-pressure gradient boundary-layers. Then, the fully coupled zonal RANS-LES approach is compared with a corresponding full domain LES for a transonic flow over the DRA2303 profile. The LES and the zonal RANS-LES approach, respectively, were chosen since RANS simulations have not yielded satisfactory results in this particular buffet case [12].

2 Mathematical formulation

2.1 Numerical methods

The Navier-Stokes equations for three-dimensional compressible flows are solved by a block-structured finite-volume flow solver. A modified AUSM method that was introduced by Liou *et al.* [13] is used for the Euler terms which are discretized to second-order accuracy by an upwind-biased approximation. For the non-Euler terms a centered approximation of second-order accuracy is used. The temporal integration from time level n to $n+1$ is done by a second-order accurate explicit 5-stage Runge-Kutta method, the coefficients of which are optimized for maximum stability. For a detailed description of the flow solver the reader is referred to Meinke *et al.*[14].

The subgrid scale modelling for the large-eddy simulations is based on an implicit ansatz, i.e., the MILES (monotone integrated LES) approach of Boris *et al.* [15] is used.

For the RANS computations the Spalart-Allmaras turbulence model [16] was chosen to close the Reynolds-averaged Navier-Stokes equations.

2.2 Synthetic turbulence generation methods (STGM)

A proper coupling of RANS and LES flow domains is considered to constitute the key feature of a zonal RANS/LES approach. In order to keep overlapping regions of both computational domains as small as possible, effective mechanisms for turbulence generation have to be applied in LES inflow regions. The turbulent characteristics coming from the RANS domain are introduced first at the LES inflow plane via synthetic turbulent eddies (Jarrin *et al.* [6], Batten *et al.* [9]) and controlled further downstream by employing control planes according to Spille and Kaltenbach [11]. The synthetic turbulence generation methods of Jarrin *et al.* and Batten *et al.* were implemented and tested for incompressible and compressible flows.

Method of Jarrin *et al.* The method of Jarrin *et al.* [6] is based on the considering of turbulence as a superposition of coherent structures. These structures are generated over the LES inlet plane and are defined by a shape function which describes the spatial and temporal characteristics of the turbulent structure.

The shape function f_σ that has a compact support on $[-\sigma, \sigma]$ where σ is a length scale which satisfies the normalization condition

$$\frac{1}{\Delta}\int_{-\Delta/2}^{\Delta/2} f_\sigma^2 \, dx \; = \; 1 \tag{1}$$

where Δ defines the extent of the domain. A one component velocity signal can then be described by the sum of the contribution $u^{(i)}(x)$ of a turbulent spot i to the velocity field. Let N be the number of prescribed synthetic eddy cores at the inlet and ϵ_i is a random number within the interval from -1 to $+1$ then the one-dimensional velocity fluctuation component reads

$$u_j'(x,t) \; = \; \frac{1}{\sqrt{N}} \sum_{i=1}^{N} \epsilon_i f_\sigma \; (x - x_i) \; . \tag{2}$$

The generalization of the one-dimensional procedure to time dependent two-dimensional fluctuations is straight forward.

Turbulent length and time scales are determined by the Reynolds shear stress component $\langle u'v' \rangle$ and the turbulent viscosity ν_t; both are extracted from corresponding RANS simulations. In this work, the Spalart-Allmaras turbulence model [16] was used for the incoming RANS solution. The turbulent time scale can be written as $t = k/\epsilon$ and the turbulent length scale as $L = t \; V_b$ with $V_b = \sqrt{k}$ where k and ϵ stand for the turbulent kinetic energy and turbulent dissipation, respectively. By applying the experimental correlation of Bradshaw *et al.* the turbulent kinetic energy is related to the Reynolds shear stress $\langle u'v' \rangle$ and the turbulent viscosity ν_t which is available from the RANS solution

$$|-\langle u'v' \rangle| = \nu_t \left| \frac{\partial u}{\partial y} \right| = a_1 \, k \tag{3}$$

with $a_1 = \sqrt{c_\mu}$ and $c_\mu = 0.09$. The turbulent dissipation ϵ is approximated by the definition of the eddy viscosity from the $k - \epsilon$ turbulence model (Menter [17])

$$\epsilon = c_\mu \, \frac{k^2}{\nu_t} \; . \tag{4}$$

The final flow field at the inlet is constructed from the resulting vortex field of Eq. 2

$$u_i = \overline{u_i} + a_{ij} u'_j \quad (5)$$

where a_{ij} is computed from the prescribed Reynolds stress tensor applying a Cholesky decomposition.

Method of Batten *et al.* The second method was introduced by Batten *et al.* [9] based on the work of Smirnov [8] and initially developed by Kraichnan [7]. To create a three-dimensional, unsteady velocity field at the inflow plane of the LES region, velocity components are constructed using a sum of sines and cosines with random phases and amplitudes. The intermediate velocity, v_i, reads

$$v_i\left(x_j.t\right) = \sqrt{\frac{2}{N}} \sum_{n=1}^{N} \left[p_i^n \cos\left(\hat{d}_j^n \hat{x}_j^n + \omega^n \hat{t}\right) + q_i^n \sin\left(\hat{d}_j^n \hat{x}_j^n + \omega^n \hat{t}\right)\right] , \quad (6)$$

where $\hat{x}$ are spatial coordinates being normalized by turbulent length- and time scales. These scales are reconstructed from the incoming RANS solution via Eqs. 3 and 5. The amplitudes of the signal are calculated by

$$p_i^n = \epsilon_{ijk} \zeta_j^n d_k^n, \qquad q_i^n = \epsilon_{ijk} \xi_j^n d_k^k \quad (7)$$

where ξ and ζ are equal to $N\left(0,1\right)$ and $\hat{d}_j^n = d_j^n V/c^n$. The wave number $d_i^n = N\left(0, 0.5\right)$ is elongated by the following relation according to Batten [9]:

$$c^n = \sqrt{\frac{3}{2} \left\langle u'_l u'_m \right\rangle \frac{d_l^n d_m^n}{d_k^n d_k^n}} \quad . \quad (8)$$

In Eq. 6 the random frequencies ω^n are taken from the normal distribution $N\left(1,1\right)$. Like in the method of Jarrin *et al.* the synthetic turbulent fluctuation field is finally reconstructed using the Cholesky decomposition. The methods are suitable in incompressible flows. In compressible flows, however, the velocity fluctuations are coupled with the density field. Thus, Morkovin's hypothesis is applied to relate density and velocity fluctuations by assuming that the pressure fluctuations over the inflow plane are negligible

$$\frac{\rho'}{\overline{\rho}} = \left(\gamma - 1\right) M^2 \frac{u'}{\tilde{u}} \quad . \quad (9)$$

Spille-Kaltenbach control planes Synthetic turbulent methods provide a reasonable first estimate of the fluctuating turbulent velocity field at the LES inlet. Downstream of the inlet, however, many of the relevant turbulent scales may have been dissipated retarding the transition to fully turbulent flow. Local control planes which introduce a volumetric forcing term to the Navier-Stokes equations regulate the turbulent production in the shear stress budget [11]. As discussed, for example, in the work of Keating *et al.* [10] or Zhang *et al.* [18], local flow events such as bursts and sweeps are enhanced or damped by the local forcing thus contributing to the Reynolds shear stress $\langle u'v' \rangle$

$$e\left(y,t\right) = \left\langle u'v' \right\rangle^{*}\left(x_0, y\right) - \left\langle u'v' \right\rangle^{z,t}\left(x_0, y, t\right) \quad (10)$$

where $\langle u'v' \rangle^{*}$ is the target Reynolds shear stress at the control plane which is provided by the RANS solution and $\langle u'v' \rangle^{z,t}$ is the current Reynolds shear stress in the LES domain which is averaged over the spanwise direction and time. For the time average a window function with a time constant equal to $\approx 100\delta_0/u_\delta$ is used.
The force magnitude is given by

$$f\left(x_0, y, z, t\right) = r\left(y,t\right)\left[u\left(x_0, y, z, t\right) - \left\langle u \right\rangle^{z,t}\right] \quad (11)$$

with

$$r\left(y,t\right) = \alpha e\left(y,t\right) + \beta \int_0^t e\left(y,t'\right) dt' \quad . \quad (12)$$

The proportional part is the main contributor to the force when the error e in Eq. 10 is high at the beginning of the simulation. Proceeding in time, the integral part gives the force the necessary response to enhance or damp the local flow events. The constants α and β were set to 10 and 25 respectively, to ensure on the one hand, a rapidly decreasing error e and on the other hand, a stable simulation process. In subsequent sections the STGM of Jarrin *et al.* combined with the control plane approach is referred to as 'zonal I' and the STGM of Batten *et al.* combined with the control plane approach is referred to as 'zonal I'.

3 Results

3.1 Validation of STGM

A zero-pressure gradient boundary-layer was investigated and compared to reference solutions using two synthetic turbulence methods, based on the controlled forcing approach downstream of the inlet. Four simulations were carried out: a full domain LES (referred as to 'full LES'), a full domain RANS, and two synthetic turbulence-LES simulations with controlled forcing. All four cases were computed with the same flow and numerical configuration, $M_\infty = 0.4$, $Re_{\delta_0} = 10000$ where δ_0

refers to the boundary layer thickness at the inlet of the computational domain. The numerical details are given in Tab. 1.
The reference full LES was computed using the rescaling method according to El-Askary *et al.* [19]. The full domain RANS calculation based on the Spalart-Allmaras model (referred to as 'RANS S-A') was performed for comparison purposes and to provide the target data for the synthetic turbulence inlet and for the control planes. In the zonal simulations the control planes are distributed over a length of one boundary-layer thickness δ_0.

Figure 1 (left) compares the evolution of the wall friction coefficient c_f for all four flow cases. The solutions of full LES and full RANS do not differ much regarding the wall shear stress for this simple zero-pressure gradient boundary-layer. Thus, the applied rescaling method at this numerical configuration is valid for LES and RANS simulations and poses no difficulty to match them at the beginning of the computational domain. Both, the zonal I and the zonal II approach, show, despite their fundamental differences in their formulations, a comparable required length until they converge to the full LES solution. The van Driest velocity profiles obtained at $x/\delta_o = 5$ which are presented in Fig. 1 (right) show that both STGM produce the expected asymptotic near-wall behavior of a turbulent flow, but the results differ somewhat at the edge of the boundary-layer.

Figure 2 depicts the turbulent kinetic energy k and Reynolds shear stress component $\langle u'v' \rangle$ at two different locations downstream of the inlet. It is shown that the flow generated by the zonal II approach undergoes a slight laminarization process downstream of the interface but the control planes increase the turbulent shear stress budget to the full LES level. The turbulent structures generated by the zonal I approach do not dissipate downstream of the inlet but the control planes introduce a local overshoot of the turbulence level which decreases to the full LES turbulence level at around five boundary-layer thicknesses δ_0.

λ_2-contours (Jeong *et al.* [20]) of both zonal cases and the full LES are visualized in Fig. 3. It is shown that the structures which are introduced into the domain by the zonal I approach are not dissipating. The structures at the inlet of the case computed with the zonal II approach fade away and the control planes downstream of the inlet have to enhance the locally rare events like turbulent bursts and sweeps to reach the turbulence level of the full LES computation.

Due to the low Reynolds number for this case it was expected that the 'artificial' turbulence would dissipate at the beginning of the domain to develop 'physical' turbulence further downstream after the transition process at about $x/\delta_0 \approx 10$. However, Figs. 1 (left) and 2 (left) show that when the zonal I approach is used the Reynolds shear stress $\langle u'v' \rangle$ does not decrease below the level of the full domain LES but generates an overshoot of turbulent kinetic energy. The zonal II approach tends to provide a lower Reynolds shear stress level which is to be increased by the control planes which are located downstream of the inlet. For the following computations the zonal I approach is used since the quality of the results is acceptable and it is computationally less expensive than the zonal II approach.
A compressible zero-pressure gradient boundary-layer ($Ma = 2.4$, $Re_{\delta_0} = 52000$) was also investigated to evaluate the efficiency of STGM in compressible flows. A full LES simulation was used as reference and a full RANS simulation provided targets for the zonal RANS-LES solution. In this case just the zonal I approach was used and evaluated concerning two different control plane configurations. The first configuration uses one single control plane (referred as to '1 c-p') which is located at $x/\delta_0 = 0.7$. The second configuration applies four control planes (referred as to 4 c-p) which are located between $x/\delta_0 = 0.3$ and $x/\delta_0 = 2$. Numerical details are given in Tab. 2.

The downstream evolution of the skin friction coefficient c_f is shown in Fig. 4 (left). It seems that the zonal I solution with one control plane already converges at about $x/\delta_0 = 1.5$ whereas the case with four control planes still regulates the shear stress budget. However, Fig. 5 compares the turbulent kinetic energy k and Reynolds shear stress $\langle u'v' \rangle$ at position $x/\delta_0 = 1$. A second spurious peak is exhibited at $y/\delta_0 = 0.7$ for the zonal I simulation with one control plane. This distribution of turbulence energy is due to the presence of a low frequency mode which is introduced at the inlet and may survive at least the first control plane. Touber *et al.* [21] observed the same phenomenon when applying synthetic turbulence techniques to compressible boundary-layers. This might occur due to the high Reynolds and Mach numbers used here which stabilizes the outer mode. However, this mode was not found in subsonic boundary-layers. When four control planes are used the flow already passes two control planes and the spurious peak in the wake region of the boundary-layer at position $x/\delta_0 = 1$ is somewhat more damped. At position $x/\delta_0 = 5$ both control plane configurations show no trace of this second peak in the turbulent kinetic energy k. From these results it is suggested to apply more than one control plane in supersonic boundary- layers at high Reynolds numbers to avoid the large wave length mode introduced by the STGM and thus to keep the tran-

sition region as small as possible. The van Driest velocity profiles obtained at $x/\delta_o = 5$ in Fig. 4 (right) show that both STGM produce the expected asymptotic near-wall behavior of a turbulent flow, but the results differ somewhat at the edge of the boundary-layer.

3.2 DRA2303 transonic profile

The DRA2303 transonic airfoil [22] was chosen as the aerodynamic reference case for the buffet phenomenon. Associated with buffet are self-sustained shock wave oscillations on airfoils at transonic flow. The flow configuration, which was to lie well within the buffet boundaries, was chosen with $Ma = 0.72$, $Re = 2.6 \cdot 10^6$ and $\alpha = 3°$. The flow configuration was chosen accordingly to available experiments that were recently conducted at the AIA Trisonic wind tunnel.

In this work the buffet is computationally targeted with three different simulations: a full domain LES which constitutes the reference solution and a fully coupled zonal RANS-LES solution. First, the RANS solution is compared with the full domain LES results of the DRA2303 airfoil and then, a fully coupled zonal RANS-LES solution yielding preliminary results is presented.

A grid resolution was chosen for the full LES and the LES domain of the zonal RANS-LES simulation according to the experience of Zhang *et al.* [18]. The numerical details of the full LES solution and the zonal RANS-LES are given in Tab. 3 and Tab. 4, respectively. The number of required grid points for the zonal RANS-LES simulation contains less than 50 $\%$ of the grid points used in the full domain LES simulation.

A full LES simulation was set up to examine the physical aspects of buffet phenomenon without using standard turbulence models. The simulation time for this configuration was about $40c/U_\infty$ which can be considered as a long term simulation where effects of initial perturbations or flow developing effects possess no influence anymore on the solution and a periodic flow behavior determines the result.

In Fig. 7 the instantaneous pressure coefficient c_p and the average pressure coefficient fluctuations at the upper side of the profile are presented. Note that the extension of the horizontal shock oscillation is $a \approx 0.07c$. The peak in the average pressure fluctuations is pronounced at about $x/c = 0.55$ and near the trailing edge the intensity of the fluctuations increases but they never exceed the strength of the shock.

The reduced frequency ω^* of the lift coefficient oscillation of the full LES solution presented in Fig. 8 is about 0.74. Oscillation of the lift coefficient is highly periodic which is indicated by the peak in the frequency spectrum. The amplitude of the lift coefficient is $\Delta C_L \approx 0.03$.

Figure 9 compares the fluctuating pressure intensity at different locations. At the upper side at $0.25c$ the amplitude of the fluctuation is very low, however, a small distinctive bump is evident at $\omega^* \approx 0.7$. Near the shock at $0.55c$ a peak occurs at the reduced frequency $\omega^* = 0.74$ and the distribution of the values is very similar to that in Fig. 8. Close to the trailing edge at $0.9c$ the major peak is still at $\omega^* \approx 0.73$ but the pressure fluctuations at higher reduced frequencies have grown stronger compared to the position near the shock. This is due to the turbulent shear layer which is at this flow configuration maximum in size at the trailing edge. Although the pressure fluctuations are averaged in the spanwise direction the pressure fluctuations at very high reduced frequencies can be related to the turbulent shear layer. At the lower side of the profile at $0.9c$ the intensity level of the fluctuations is one order of magnitude smaller compared with the corresponding position at the upper side. However, a distinct peak at $\omega^* \approx 0.73$ is visible which is caused by the direct influence of the oscillating shock at the upper side.

The Reynolds shear stresses of the averaged full LES solution at two different locations is exhibited in Fig. 6. At 0.4 c the distribution resembles that of a flat plate boundary-layer flow and its turbulent features. Behind the shock, however, the maxima of all components moves to the center of the boundary-layer and the intensity level of $\langle v'v' \rangle$, $\langle w'w' \rangle$, and $\langle u'v' \rangle$ is much higher compared with the position ahead of the shock. Downstream of the shock the intensities of $\langle u'u' \rangle$, $\langle v'v' \rangle$, and $\langle w'w' \rangle$ are at the same level which indicates that the turbulent structures show an isotropic behavior compared with the high level of anisotropy of the near-wall turbulence upstream of the shock.

The λ_2-contours [20] are shown in Fig. 10. After the interaction with the shock, the turbulent boundary-layer separates and a shear flow is formed that develops large coherent structures that convect near the trailing edge. These large structures are responsible for the high level pressure oscillations at high frequencies near the trailing edge.

The experimental findings showed a horizontal shock amplitude at the upper side of the airfoil of $a_{exp} \approx 0.05c$ with a corresponding reduced frequency of $\omega^*_{exp} = 0.68$. Hence, the full LES results regarding buffet dynamics agree well with the available experimental data ($a_{num} \approx 0.07c$ and $\omega^*_{num} = 0.74$).

In order to analyze the buffet phenomenon with

a higher order turbulence model, i. e. a local LES, and to use a global efficient Ansatz the zonal RANS-LES approach was applied. The computational set up is shown in Fig. 11. The Spalart-Allmaras turbulence model [16] was used to close the RANS equations of the zonal RANS-LES approach. Due to the complexity of this particular case the results can be considered just preliminary.

RANS and LES domains used periodic boundary conditions in the spanwise direction and a no-slip, adiabatic condition was set at the wall. Non-reflective boundary conditions were applied at the far field boundaries. At the inlet of the LES domain on the upper and lower side of the airfoil, the zonal I approach according to Jarrin *et al.* [6] (see section 2.2) was used to generate synthetic turbulent structures. Downstream of the inlet four control planes are located between $0.37c$ and $0.4c$ at the upper side and between $0.7c$ and $0.73c$ at the lower side of the airfoil. The turbulent flow properties of the upstream RANS solution were used as target conditions for the zonal I approach and the control planes that were located downstream of the LES inlet. At the LES outlet the method of König *et al.* [23] was employed to reconstruct the required turbulent viscosity ν_t for the RANS domain that is located downstream of the LES region. At the RANS outflow a time averaged pressure from the LES domain located downstream is prescribed whereas density and velocity profiles are extrapolated. At the LES inflow the density and velocity profiles are transferred from the RANS domain located upstream and the pressure is extrapolated from the interior of the LES-domain. The term 'fully coupled' refers to the above mentioned treatment of the in- and outflow boundaries of the RANS and LES domains. The LES domain is surrounded by a sponge layer to damp pressure fluctuations that otherwise might be reflected at the boundaries. Further details of such a sponge layer are given in [18].

Since pressure waves, caused by the transient shock behavior , travel from the LES domain to the RANS domain and vice versa the time window where the solutions are averaged has to be carefully defined. On the one hand, the turbulent flow properties of the LES solution have to be averaged properly over a sufficiently large time window before being transferred to the RANS domain. On the other hand, the amplitude and frequency of the traveling pressure waves caused by the shock must be captured in a time window which is as small as possible to prevent a significant alteration of the pressure wave signal. A time window of the size of 1 c/U_∞ was found to satisfy these requirements .

In Fig. 12 the instantaneous pressure coefficients c_p are given. The zonal RANS-LES solution shows a good agreement with the full LES solution concerning shock position and strength. Downstream of the shock the c_p evolution shows minor discrepancies near the trailing edge. However, upstream of the shock the zonal RANS-LES results agree pretty well with the findings of the full LES. Note the smooth transition from RANS to LES of the pressure coefficient near the overlapping zones at approximately $0.37c$ (upper side) and $0.7c$ (lower side).

The λ_2-contours of the instantaneous zonal RANS-LES solution are depicted in Fig. 13. They show the same features compared to the contours of the full LES simulation such as large coherent structures downstream of the shock interaction zone convecting towards the trailing edge.

4 Conclusion

In this article, different inflow conditions for zonal RANS-LES simulations at the LES inlet where evaluated and compared. To couple the RANS with the LES domain, synthetic turbulence generating approaches and control planes were used to prescribe the turbulent intensities of the RANS solution for the LES domain. Two different STGM were tested and validated for a subsonic zero-pressure gradient boundary-layer flow. The zonal I approach was found to be superior compared to the zonal II approach and therefore used in subsequent computations.

The application of two different control plane configurations in a supersonic zero-pressure gradient boundary-layer flow showed similar as in [21], that long wave oscillations are generated, which disturb the solution, if only one control plane is used. Such disturbances can be removed by using several control planes.

Finally, the zonal RANS-LES was applied to simulate the transonic flow around a DRA2303 airfoil. The results of a pure LES long term simulation agreed well with experimental findings. The coupled zonal RANS-LES approach provided preliminary results which indicate that the quality of the solution is comparable to that of the full domain LES solution. The computational costs could be reduced by a factor of 2 for this case.

References

[1] D. C. Wilcox, Turbulence Modeling for CFD, DCW Industries, 1993.

[2] J. Fröhlich, D. v. Terzi, Hybrid les/rans methods for the simulation of turbulent flows, Prog. Aerospace Sci. 44 (2008) 349–377.

[3] P. R. Spalart, W. H. Jou, M. Strelets, S. R. Allmaras, Comments on the feasibility of les for wings, and on a hybrid rans/les approach, Advances on DNS/LES, Greyden Press, Columbus, OH, 1997.

[4] K. D. Squires, Detached-eddy simulation: current status and perspectives, Direct and Large-Eddy Simulation, Kluwer, Dordrecht, 2004, pp. 465–480.

[5] A. Keating, U. Piomelli, E. Balaras, H.-J. Kaltenbach, A priori and a posteriori tests of inflow conditions for large-eddy simulation, Physics of Fluids 16 (12) (2004) 4696–4712.

[6] N. Jarrin, S. Benhamadouche, D. Laurence, R. Prosser, A synthetic-eddy-method for generating inflow conditions for large-eddy simulations, International Journal of Heat and Fluid Flow 27.

[7] R. H. Kraichnan, Inertial Ranges in Two-Dimensional Turbulence, Physics of Fluids 10 (7) (1967) 1417 – 1423.

[8] A. Smirnov, S. Shi, I. Celik, Random flow generation technique for large eddy simulations and particle dynamics modeling, Journal of Fluids Engineering 123.

[9] P. Batten, U. Goldberg, S. Chakravarthy, Interfacing statistical turbulence closures with large-eddy simulation, AIAA Journal 42 (3) (2004) 485–492.

[10] A. Keating, G. de Prisco, U. Piomelli, Interface conditions for hybrid rans/les calculation, International Journal of Heat and Fluid Flow 27.

[11] A. Spille, H.-J. Kaltenbach, Generation of turbulent inflow data with a prescribed shear-stress profile, 2001, third AFSOR Conference on DNS and LES.

[12] W. Wagner, An Experimental Investigation of Passive Shock/Boundary Layer Interaction Control on an Airfoil: Unsteady Measurements, in: E. H. Hirschel (Ed.), EUROSHOCK. drag reduction by passive shock control; results of the project EUROSHOCK, Vol. 36 of Notes on Numerical Fluid Mechanics, Vieweg Verlag, Braunschweig, 1997, pp. 401–414.

[13] M.-S. Liou, C. J. Steffen, A new flux splitting scheme, Journal of Computational Physics 107 (1993) 23–39.

[14] M. Meinke, W. Schröder, E. Krause, T. Rister, A comparison of second- and sixth-order methods for large-eddy simulations, Computers and Fluids 31 (2002) 695–718.

[15] J. P. Boris, F. F. Grinstein, E. S. Oran, R. L. Kolbe, New insights into large eddy simulation, Fluid Dynamics Research 10 (1992) 199–228.

[16] P. R. Spalart, S. R. Allmaras, A One-Equation Turbulence Model for Arodynamic Flows, Paper 92-0439, AIAA, 30th Aerospaace Sciences Meeting & Exhibit, Jan 6-9, Reno (1992).

[17] F. R. Menter, Eddy viscosity transport equations and their relation to the $k-\epsilon$-model, Journal of Fluids Engineering 119 (1997) 876–884.

[18] Q. Zhang, W. Schröder, M. Meinke, A zonal rans/les method to determine the flow over a high-lift configuration, Accepted for publication in Computers and Fluids.

[19] W. A. El-Askary, M. Meinke, W. Schröder, Large Eddy Simulation of a Compressible Boundary Layer, Tech. rep., presented at GAMM conference 2002, March 25-28, Augsburg (2002).

[20] J. Jeong, F. Hussain, On the identification of a vortex, J. Fluid Mech. 285 (1995) 69–94.

[21] E. Touber, N. D. Sandham, Large-eddy simulation of low-frequency unsteadiness in a turbulent shock induced separation bubble, Theor. Comput. Fluid Dyn. 23 (2009) 79–107.

[22] J. L. Fulker, M. J. Simmons, An Experimental Investigation of Passive Shock/Boundary Layer Interaction Control on an Aerofoil, DRAIASIHWAICR 9521611 EUROSHOCK TR AER 2 4913 (2).

[23] D. König, W. Schröder, M. Meinke, Embedded les-to-rans boundary in zonal simulations, Accepted for publication in Journal of Turbulence.

Table 1: Numerical details for the simulation of a turbulent boundary layer at $Ma = 0.4$ and $Re_\delta = 10000$ for LES and RANS solutions

	streamwise x	wall normal y	spanwise z
Domain size in δ_0	15	5	0.7
Grid points	484	65	49
Resolution, wall units	$\Delta x^+ \approx 20$	$\Delta y^+_{min} \approx 0.8$	$\Delta z^+ \approx 12$

Table 2: Numerical details for the computation of a turbulent boundary layer at $Ma = 2.4$ and $Re_\delta = 52000$ for LES and RANS solutions

	streamwise x	wall normal y	spanwise z
Domain size in δ_0	10	3	0.7
Grid points	140	65	49
Resolution, wall units	$\Delta x^+ \approx 20$	$\Delta y^+_{min} \approx 0.8$	$\Delta z^+ \approx 12$

Table 3: Numerical details for the of transonic flow over the DRA2303 airfoil for a full domain LES simulation

	streamwise x	wall normal y	spanwise z
Domain size in c	20	20	0.021
Grid points ($30.4 \cdot 10^6$)	2364	130	99
Resolution, wall units	$\Delta x^+ \approx 100$	$\Delta y^+_{min} \approx 1.0$	$\Delta z^+ \approx 20$

Table 4: Numerical details of the LES domain for a zonal RANS-LES simulation of transonic flow over the DRA2303 airfoil

	streamwise x	wall normal y	spanwise z
Grid points ($13.7 \cdot 10^6$)	1430	97	99
Resolution, wall units	$\Delta x^+ \approx 100$	$\Delta y^+_{min} \approx 1.0$	$\Delta z^+ \approx 20$

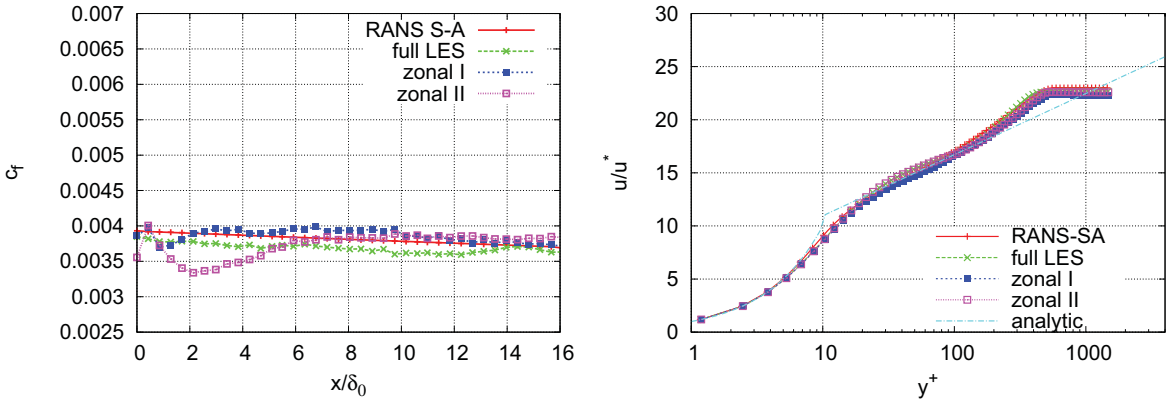

Figure 1: Evolution of skin friction coefficient c_f (left) and van Driest velocity profile (right) for boundary layer flow at $Ma = 0.4$ and $Re_{\delta_0} = 10000$ for different computational configurations $x/\delta_0 = 5$

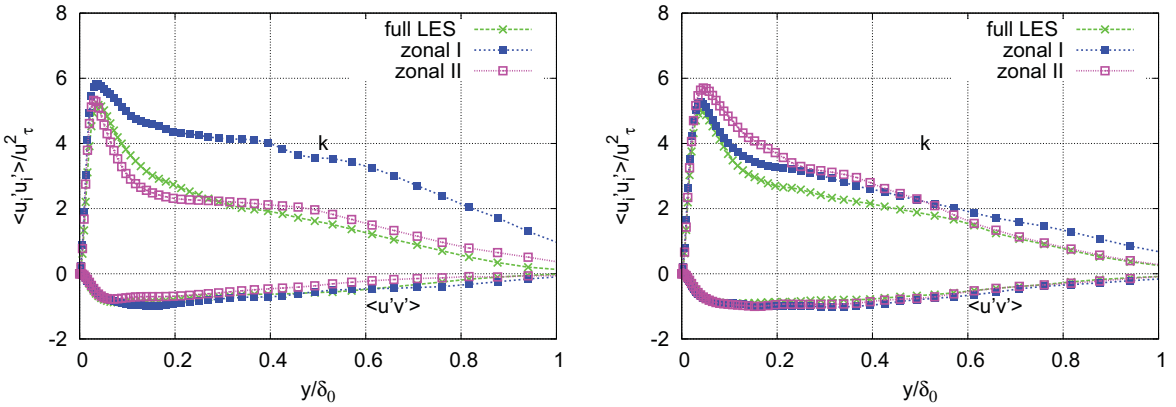

Figure 2: Turbulent kinetic energy k and Reynolds shear stress $\langle u'v' \rangle$ at $x/\delta_0 = 1$ (left) and at $x/\delta_0 = 5$ (right) for a full domain LES and a zonal RANS-LES computation

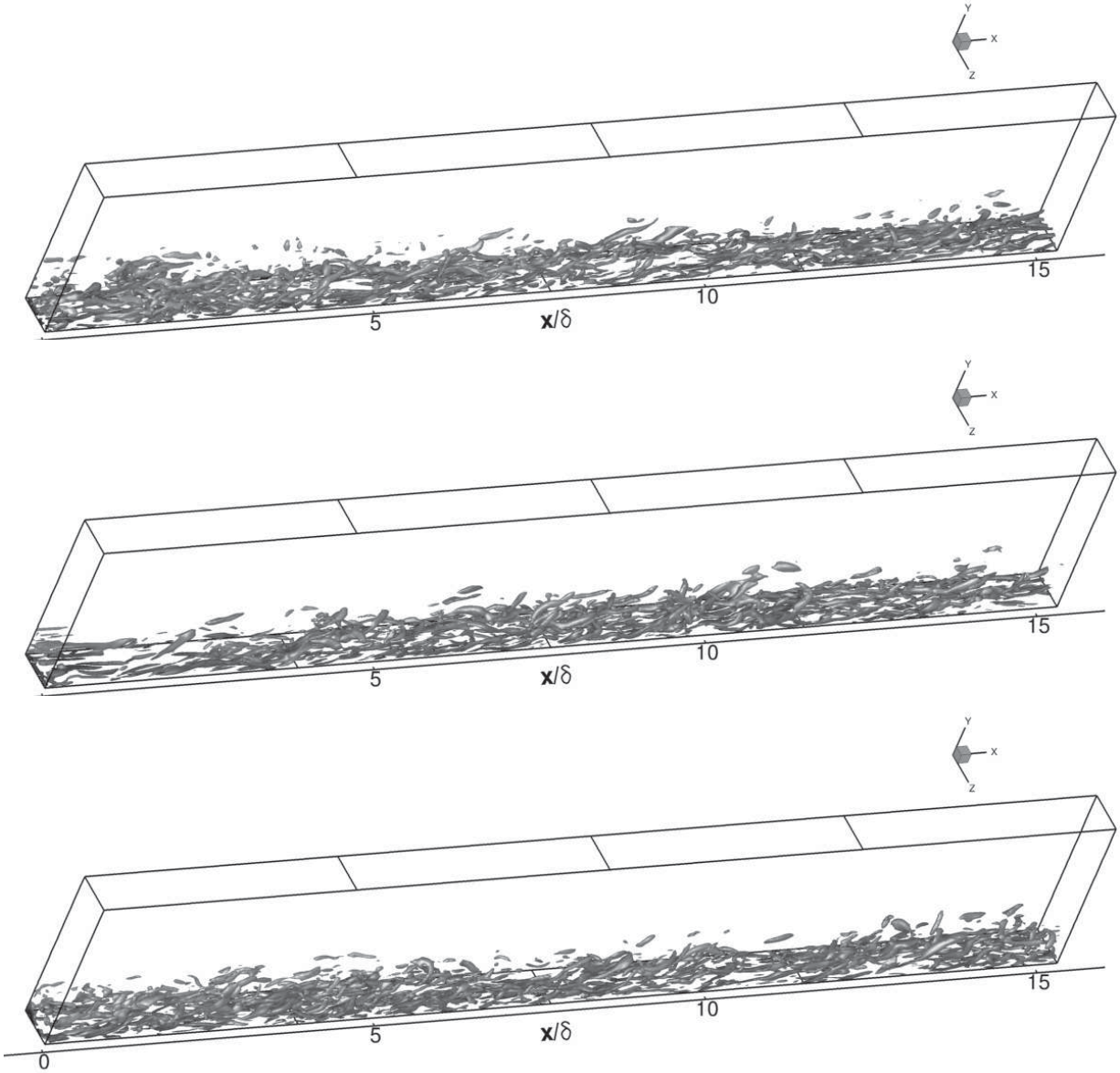

Figure 3: λ_2 structures of a mildly compressible flat plate boundary layer flow computed by (top) a full LES, (middle) using zonal II approach and (bottom) applying the zonal I ansatz

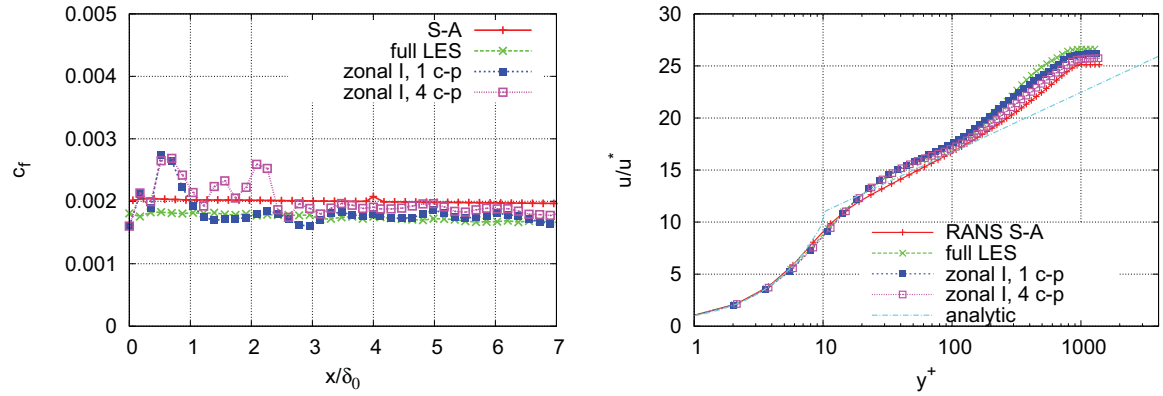

Figure 4: Evolution of skin friction coefficient c_f (left) and van Driest velocity profile (right) for boundary layer flow at $Ma = 2.4$ and $Re_{\delta_0} = 52000$ for different computational- and control plane configurations at $x/\delta_0 = 5$

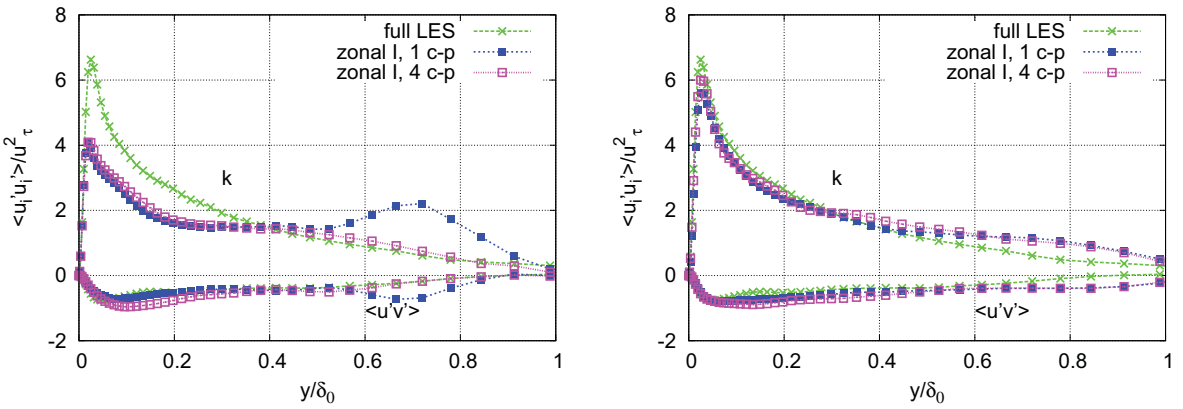

Figure 5: Turbulent kinetic energy k and Reynolds shear stress $\langle u'v' \rangle$ at $x/\delta_0 = 1$ (left) and at $x/\delta_0 = 5$ (right) for a full domain LES and a zonal RANS-LES computation

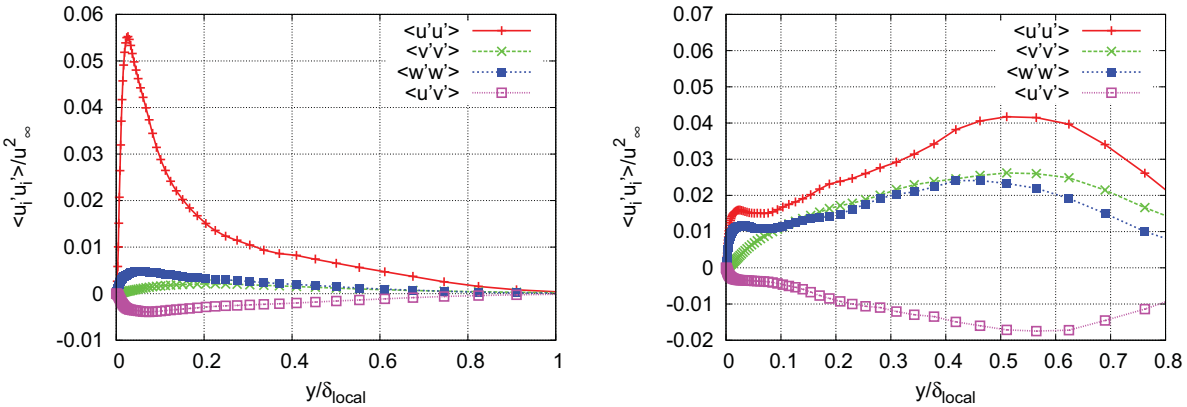

Figure 6: Reynolds shear stresses of a full LES at two different positions at the DRA2303-profile: at $x/c = 0.4$ (left) and $x/c = 0.6$ (right)

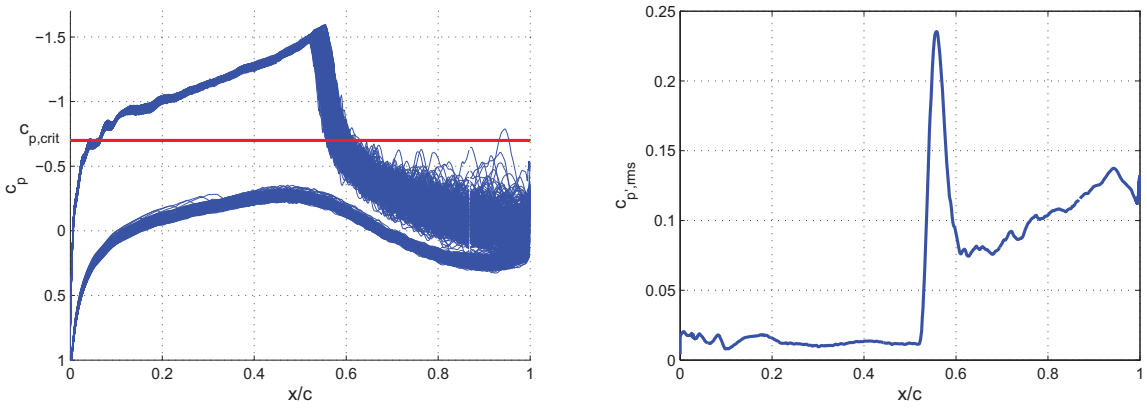

Figure 7: Fluctuating wall pressure coefficient c_p (left) and corresponding rms-values at the upper side of the profile (right) for a full LES computation

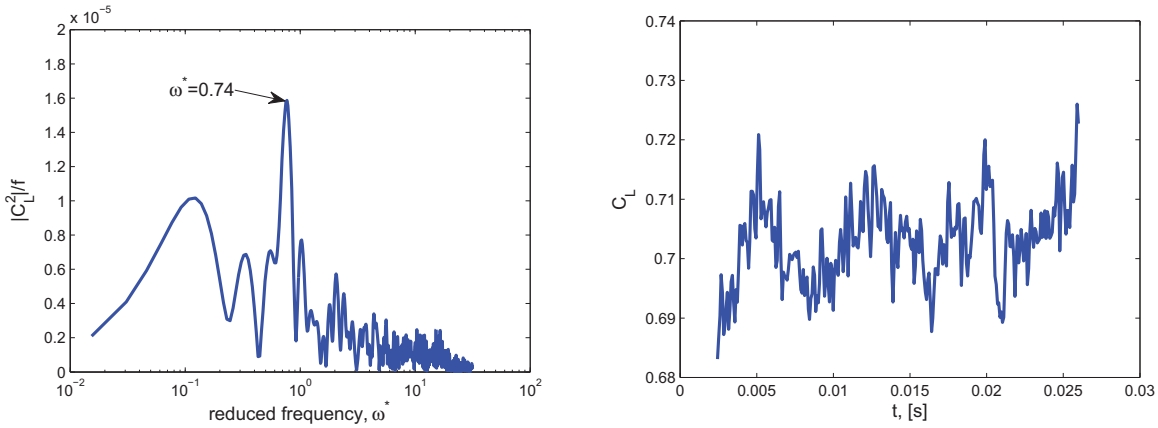

Figure 8: Power spectral density of fluctuations of lift coefficient C_L and corresponding fluctuations over time for the full domain LES of a transonic flow around a DRA2303 airfoil

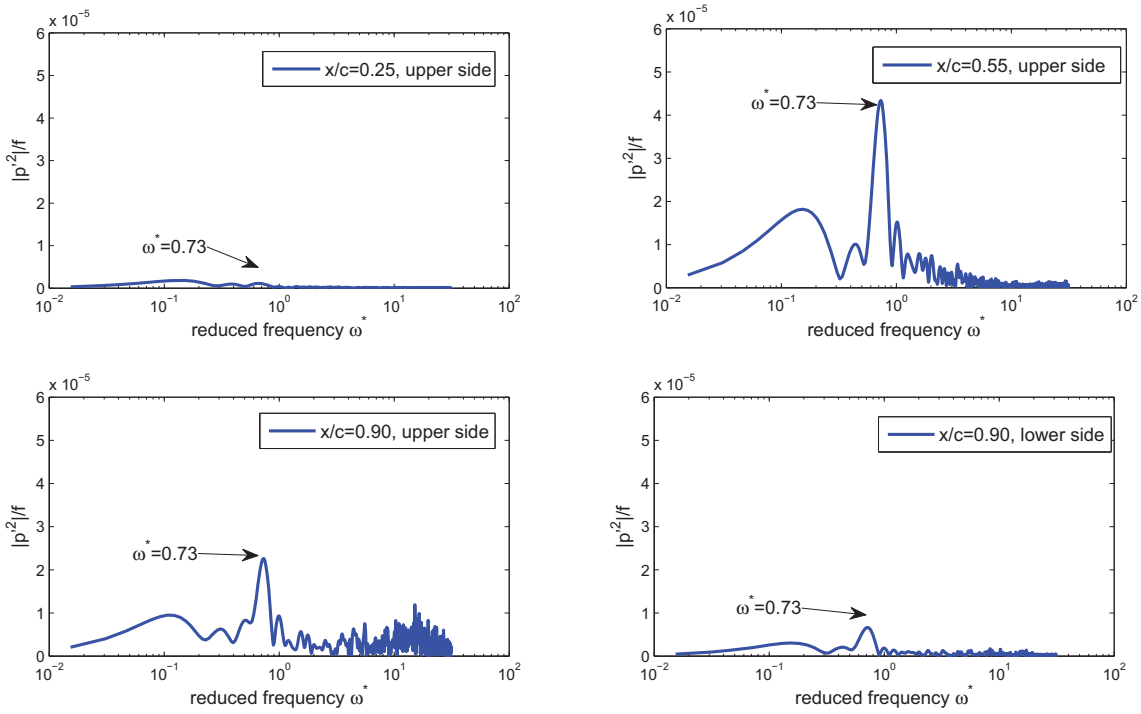

Figure 9: Power spectral density of pressure fluctuations computed by a full domain LES at different positions of the DRA2303-airfoil

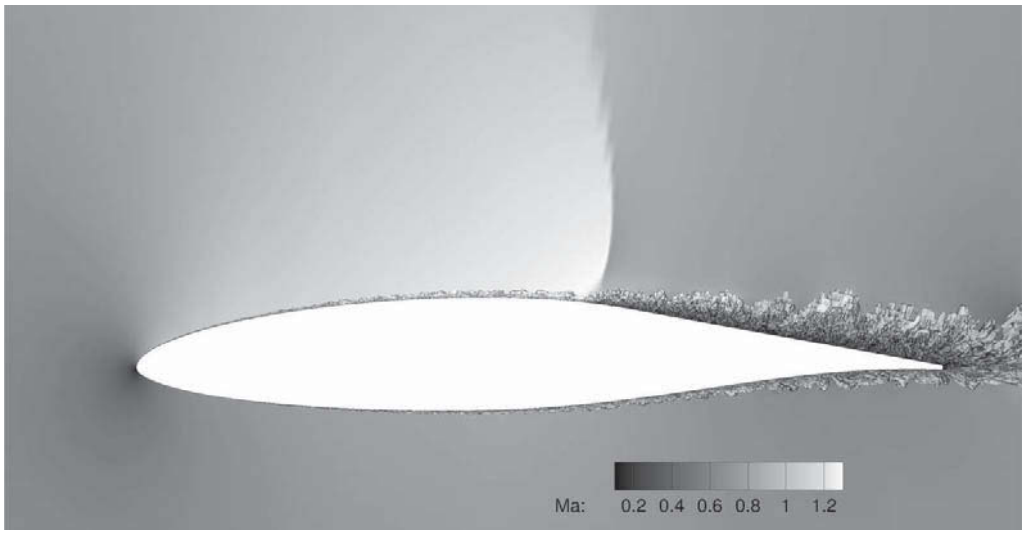

Figure 10: λ_2 structures of transonic flow around a DRA2303 profile for a full domain LES simulation

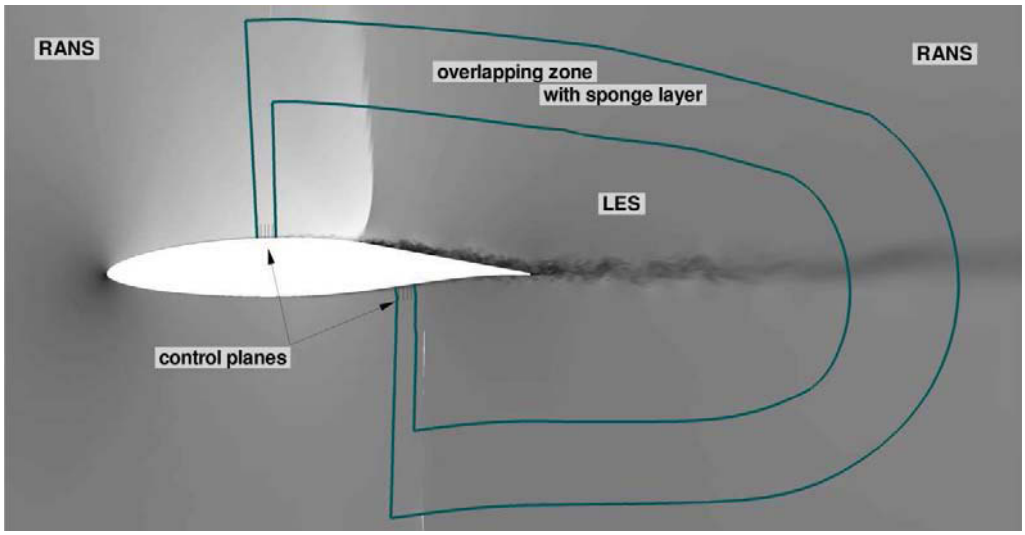

Figure 11: Computational setup of a fully coupled zonal RANS-LES simulation of a transonic flow around a DRA2303 airfoil

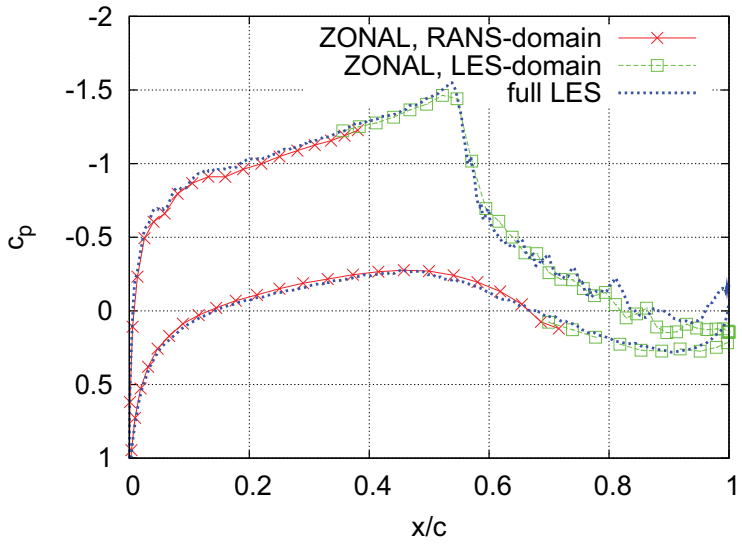

Figure 12: Comparison of instantaneous pressure coefficient c_p between full domain LES and zonal RANS-LES computation of a transonic flow around a DRA2303 airfoil

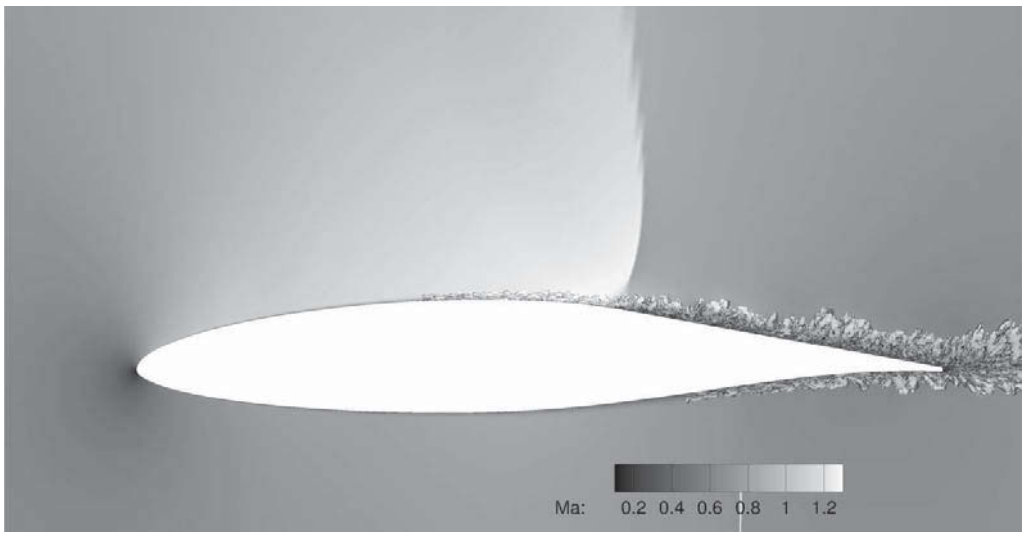

Figure 13: λ_2 structures of transonic flow around a DRA2303 airfoil for a fully coupled zonal RANS-LES solution